


# Effects of dark matter on the nuclear and neutron star matter

H. C. Das<sup>1,2</sup> \*, Ankit Kumar<sup>1,2</sup>, Bharat Kumar<sup>3</sup>, S. K. Biswal<sup>4</sup>,  
Takashi Nakatsukasa<sup>3</sup>, Ang Li<sup>4</sup>, S. K. Patra<sup>1,2</sup>,

<sup>1</sup> *Institute of Physics, Sachivalya Marg, Bhubaneswar-751005, India*

<sup>2</sup> *Homi Bhabha National Institute, Training School Complex, Anushakti Nagar, Mumbai 400085, India*

<sup>3</sup> *Center for Computational Sciences, University of Tsukuba, Tsukuba 305-8577, Japan*

<sup>4</sup> *Department of Astronomy, Xiamen University, Xiamen 361005, P. R. China*

29 November 2021

## ABSTRACT

We study the dark matter effects on the nuclear matter parameters characterising the equation of states of super dense neutron-rich nucleonic-matter. The observables of the nuclear matter, i.e. incompressibility, symmetry energy and its higher-order derivatives in the presence dark matter for symmetric and asymmetric nuclear matter are analysed with the help of an extended relativistic mean-field model. The calculations are also extended to  $\beta$ -stable matter to explore the properties of the neutron star. We analyse the dark matter effects on symmetric nuclear matter, pure neutron matter and neutron star using NL3, G3 and IOPB-I forces. The binding energy per particle and pressure are calculated with and without considering the dark matter interaction with the nuclear matter systems. The influences of dark matter are also analysed on the symmetry energy and its different coefficients. The incompressibility and the skewness parameters are affected considerably due to the presence of dark matter in the nuclear matter medium. We extend the calculations to the neutron star and find its mass, radius and the moment of inertia for static and rotating neutron star with and without dark matter contribution. The mass of the rotating neutron star is considerably changing due to rapid rotation with the frequency in the mass-shedding limit. The effects of dark matter are found to be important for some of the nuclear matter parameters, which are crucial for the properties of astrophysical objects.

**Key words:** dark matter– equation of state– stars: neutron

## 1 INTRODUCTION

It is well known that our Universe has only  $\sim 6\%$  visible matter and the remaining  $\sim 94\%$  is considered to be dark matter (DM) and dark energy. Zwicky estimated the total mass of the Universe (Zwicky 2009; Kouvaris & Tinyakov 2010) and found that something is missing, which are termed as DM ( $\sim 26\%$ ) and dark energy ( $\sim 68\%$ ). Many theoretical, experimental and observational efforts have been put to know the mystery of DM and dark energy. Several DM candidates are hypothesized, like weakly interacting massive particles (WIMPs) (Kouvaris & Tinyakov 2011; Quddus et al. 2019), feebly interacting massive particles (FIMPs) (Bernal et al. 2017; Hall et al. 2010), Neutralino (Hooper & Wang 2004; Han et al. 2014; Das et al. 2019) and axions (Duffy & van Bibber 2009) etc. The WIMPs are expected to produce in the early hot Universe and annihilate in pairs, and these are the thermal relics of the Universe (Ruppin et al. 2014). The WIMPs might have decayed in the dense region of the Universe to yield standard model (SM) particles, gamma rays, leptons and neutrinos. Many experiments have already been performed to find out the direct and indirect consequences of DM. The direct experimental searches like DAMA (Bernabei et al. 2008, 2010), Xenon (Angle et al. 2008) and CDMS (CDMS 2010) are set up to find the cross-section between WIMPs and nucleons. The indirect detection experiments like Fermi large area telescopes

and imaging air Cherenkov telescopes have also established (Conrad 2014). In addition to that, the effects of DM on compact stars such as neutron star (NS) and white dwarfs have been studied with different DM models (Kouvaris 2008; Bertone & Fairbairn 2008). For example, the self-annihilating DM inside the NS heat the stars, and it would affect the cooling properties of compact stars (Kouvaris 2008; Bhat & Paul 2019). On the other hand, non-self-annihilating DM is accumulated inside the stars and affects the stellar structure (De Lavallaz & Fairbairn 2010; Ciarcelluti & Sandin 2011). In this paper, we consider fermionic DM interacting with nucleonic matter via the Higgs portal mechanism and constraints the nuclear matter (NM) and NS properties through DM parameters.

To understand equation of state (EoS) of NS matter, it is imperative to analyze the NM parameters at different proton-neutron compositions ( $\alpha = \frac{\rho_n - \rho_p}{\rho_n + \rho_p}$ ), where  $\rho_n$  and  $\rho_p$  are the neutron and proton densities respectively. The NM parameters, such as binding energy per particle (BE/A), incompressibility ( $K$ ), symmetry energy ( $S$ ) and its derivatives ( $L$ -slope parameter,  $K_{sym}$ -isovector incompressibility and  $Q_{sym}$ -skewness parameter) are the key quantities for the study of an EoS. The NSs are the extreme object with a high degree of density and isospin asymmetry. Hence it is interesting to study the NM parameters at different conditions, from low to high density and at different asymmetric factor  $\alpha = 0$  to 1 in the presence of DM. In Ref. (Alam et al. 2016), it was shown that the linear combinations of the isoscalar and isovector NM parameters

\* E-mail: harish.d@iopb.res.in

are strongly correlated with NS radii over a wide range of NS mass. These correlations are particularly important for the canonical mass  $1.4M_{\odot}$  of the NS. With the help of GW170817 observation, a similar better correlation exists between the tidal deformability  $\Lambda$  and the Love number  $k_2$  with the linear combination of the  $M_0$  and the curvature of the symmetry energy  $K_{sym,0}$  at saturation density (Malik et al. 2018; Carson et al. 2019). Also, recently it is reported by various authors (Sandin & Ciarcelluti 2009; Kouvaris & Tinyakov 2010; De Lavallaz & Fairbairn 2010; Ciarcelluti & Sandin 2011; Leung et al. 2011; Li et al. 2012; Panotopoulos & Lopes 2017; Ellis et al. 2018; Bhat & Paul 2019; Das et al. 2019; Ivanytskyi et al. 2019; Quddus et al. 2019) that the NS core contains an admixture of DM including many exotic baryonic species.

The internal structure of a NS is not well known till now, so we believe many phenomena like quark deconfinement (Collins & Perry 1975; Orsaria et al. 2014; Mellinger et al. 2017), kaon condensation (Kaplan & Nelson 1988; Glendenning & Schaffner-Bielich 1998; Glendenning & Schaffner-Bielich 1999; Pal et al. 2000; Gupta & Arumugam 2012), phase transition (Glendenning 1992; Sharma et al. 2007) and hyperons production (Ambartsumyan & Saakyan 1960; Glendenning 1985; Schaffner & Mishustin 1996; Schulze et al. 2006; Dapo et al. 2010; Bhowmick et al. 2014; Biswal et al. 2016; Fortin et al. 2017; Bhuyan et al. 2017; Biswal 2019; Biswal et al. 2019) are occur inside the star. The EoS plays a vital role to predict all the star parameters such as mass ( $M$ ), radius ( $R$ ), tidal deformability ( $\Lambda$ ) and moment of inertial ( $I$ ) of the NS. Many theoretical and observational studies have been devoted to constraint these parameters. The binary NS merger event GW170817 (Abbott et al. 2017, 2018) provides a strong constraint on the EoS. The recently reported massive NS (PSR J0740+6620) (Cromartie et al. 2019) with the mass of  $2.14^{+0.20}_{-0.18} M_{\odot}$  within the 95.4% confidence limits, also puts a strong constraint on the nature of EoS.

Recently the simultaneous measurements of the  $M$  and  $R$  for NS are done by the NASA Neutron star Interior Composition Explorer (NICER) (Miller et al. 2019; Riley et al. 2019; Bogdanov et al. 2019; Bilous et al. 2019; Raaijmakers et al. 2019; Guillot et al. 2019), which constraint the EoS. For that, we extend our calculations for rotating NS to measure the  $M$ ,  $R$  and  $I$  in the presence of DM. The theoretical observations allow the Keplerian frequency of the rotating NS is more than 2000 Hz, but two fastest pulsar detected have frequencies 716 Hz (Hessels et al. 2006) and 1122 Hz (Kaaret et al. 2007). Many calculations related to the Keplerian frequencies (Stergioulas 2003; Dhiman et al. 2007; Jha et al. 2008; Krastev et al. 2008; Haensel et al. 2009; Sharma & Jha 2009; Koliogiannis & Moustakidis 2020) are devoted to fix the frequency range within this limit. In this work, we want to study the effect of mass-shedding frequency on the mass of the DM admixture NS, which can be used to constraint the EoS.

The EoS, which is the main input to the Tolman-Oppenheimer-Volkoff (TOV) equations (Tolman 1939; Oppenheimer & Volkoff 1939) determine the stable configurations of a static NS, are constructed in several ways. The non-relativistic formalism with various Skyrme parametrizations (Skyrme 1956, 1958; Vautherin & Brink 1972; Chabanat et al. 1998; Alex Brown 1998; Stone & Reinhard 2007; Dutra et al. 2012; Dechargé & Gogny 1980) and three-body potential of Akmal-Pandheripande (Akmal et al. 1998) are very successful in describing the nuclear EoS, including the NS. The relativistic mean-field (RMF) model, which gives a good description not only explains well the finite nuclei in the

$\beta$ -stability line but also reproduce the experimental data for exotic and superheavy nuclei (Rashdan 2001; Bhuyan & Patra 2012; Bhuyan 2018; Kumar et al. 2018). In the present paper, we use the extended RMF (E-RMF) models for the study of effects of DM on NM and NS properties with the well known NL3 (Lalazissis et al. 1997), G3 (Kumar et al. 2017) and IOPB-I (Kumar et al. 2018) parameter sets.

The effects of the DM on the NS have already discussed in some recent works, for example, Panotopoulos et al. (Panotopoulos & Lopes 2017), Das et al. (Das et al. 2019) and Quddus et al. (Quddus et al. 2019). But our analysis gives a better and wider platform to discuss the DM effects on the bulk properties of the NM and the NS. Here, we briefly describe their works. Panotopoulos et al. (Panotopoulos & Lopes 2017) have calculated the NS EoS with simple  $\sigma$ - $\omega$  model (Walecka 1974), and they have added the DM with static NS to find its  $M$  and  $R$ . They assumed that the DM particles interact with nucleons via SM Higgs. They considered Neutralino as a DM candidate, which has mass 200 GeV and Higgs mass is 125 GeV. Das et al. (Das et al. 2019) have taken the same RMF model but with NL3 parameter set (Lalazissis et al. 1997) and calculate the EoS,  $M$ ,  $R$  and  $\Lambda$  of the static NS. Quddus et al. (Quddus et al. 2019) have taken the E-RMF formalism, which is suitable for constraints on the properties of the NS in the presence of WIMP dark matter. The main difference between earlier two work and Quddus et al. is that they have taken light Higgs mass 40 GeV and DM mass up to 8 GeV. In the present calculations, we take three non-linear parameter sets, whose nuclear matter properties cover a wide range. Though simple  $\sigma$ - $\omega$  model gives a qualitative picture of the RMF model, still many important information are missing in the linear  $\sigma$ - $\omega$  model. But E-RMF calculation covers a full set of non-linear model contain various important interaction terms as in Refs. (Kumar et al. 2017, 2018). We add the DM with the NM and calculate NM parameters like  $BE/A$ ,  $K$ ,  $S$ ,  $L$ ,  $K_{sym}$  and  $Q_{sym}$  for the whole density range. Finally, we apply the  $\beta$ -equilibrium condition to the NM EoS. When we add the DM to the NM, we follow the same formalism by the Panotopoulos et al. Panotopoulos & Lopes (2017) and Das et al. (Quddus et al. 2019). Then we calculate the  $M$ ,  $R$  and  $I$  both for static and rotating NS and we compare both the results.

The paper is organised as follows: the formalism used in this work is presented in Sec. 2. In Sub-Sec. 2.1, we explain the basic formalism of RMF model using NL3 and the recently developed G3 and IOPB-I forces for the calculations of nucleonic EoS. In Sub-Sec. 2.2, we take the interaction of DM with NM and calculate the EoS of nucleons with DM. In Sub-Sec. 2.3, we calculate different parameters of NM. The Sub-Sec. 2.4 the calculation of EoS of NS using  $\beta$ -equilibrium and charge-neutrality conditions. In Sub-Sec. 2.5, the observables of the NS are calculated like  $M$ ,  $R$ ,  $I$  etc. for static NS (SNS) and rotating NS (RNS). The results and discussions are detailed in Sec. 3. Finally, summary and our concluding remarks are outlined in Sec. 4.

## 2 THEORETICAL FRAMEWORK

From the last four decades, the RMF approaches are extremely popular to describe finite and infinite NM properties. The Lagrangian is constructed by taking the interaction of few numbers of mesons with nucleons and their self and cross-couplings. The parameters are constructed, taking into account the experimental data of few finite nuclei, saturation properties of the infinite NM and NS properties.

## 2.1 Construction of RMF approach to find EoS for nucleons

The RMF Lagrangian is built from the interaction of mesons-nucleons and their self ( $\Phi^3, \Phi^4, W^4$ ) and cross-couplings ( $\Phi^2 - W^2, R^2 - W^2, \Phi - W^2$  and  $\Phi - R^2$ ) of the mesons fields  $\Phi, W, R, D$ . Where  $\Phi, W, R$  and  $D$  are the redefined fields for  $\sigma, \omega, \rho$  and  $\delta$  mesons as  $\Phi = g_s \sigma^0, W = g_\omega \omega^0, R = g_\rho \vec{\rho}^0$  and  $D = g_\delta \delta^0$  respectively. The RMF Lagrangian is discussed in these Refs. (Miller & Green 1972; Serot & Walecka 1986; Furnstahl et al. 1987; Reinhard 1988; Furnstahl et al. 1997; Kumar et al. 2017, 2018). The energy density ( $\mathcal{E}_{nucl.}$ ) and pressure ( $P_{nucl.}$ ) for a nucleon-meson interacting system are given as (Kumar et al. 2018; Quddus et al. 2019)

$$\begin{aligned} \mathcal{E}_{nucl.} = & \frac{\gamma}{(2\pi)^3} \sum_{i=p,n} \int_0^{k_i} d^3k E_i^*(k_i) + \rho_b W + \frac{1}{2} \rho_3 R \\ & + \frac{m_s^2 \Phi^2}{g_s^2} \left( \frac{1}{2} + \frac{\kappa_3}{3!} \frac{\Phi}{M_{nucl.}} + \frac{\kappa_4}{4!} \frac{\Phi^2}{M_{nucl.}^2} \right) - \frac{1}{4!} \frac{\zeta_0 W^4}{g_\omega^2} \\ & - \frac{1}{2} m_\omega^2 \frac{W^2}{g_\omega^2} \left( 1 + \eta_1 \frac{\Phi}{M_{nucl.}} + \frac{\eta_2}{2} \frac{\Phi^2}{M_{nucl.}^2} \right) \\ & - \Lambda_\omega (R^2 \times W^2) - \frac{1}{2} \left( 1 + \frac{\eta_\rho \Phi}{M_{nucl.}} \right) \frac{m_\rho^2}{g_\rho^2} R^2 \\ & + \frac{1}{2} \frac{m_\delta^2}{g_\delta^2} D^2, \end{aligned} \quad (1)$$

$$\begin{aligned} P_{nucl.} = & \frac{\gamma}{3(2\pi)^3} \sum_{i=p,n} \int_0^{k_i} d^3k \frac{k^2}{E_i^*(k_i)} + \frac{1}{4!} \frac{\zeta_0 W^4}{g_\omega^2} \\ & - \frac{m_s^2 \Phi^2}{g_s^2} \left( \frac{1}{2} + \frac{\kappa_3}{3!} \frac{\Phi}{M_{nucl.}} + \frac{\kappa_4}{4!} \frac{\Phi^2}{M_{nucl.}^2} \right) \\ & + \frac{1}{2} m_\omega^2 \frac{W^2}{g_\omega^2} \left( 1 + \eta_1 \frac{\Phi}{M_{nucl.}} + \frac{\eta_2}{2} \frac{\Phi^2}{M_{nucl.}^2} \right) \\ & + \Lambda_\omega (R^2 \times W^2) + \frac{1}{2} \left( 1 + \frac{\eta_\rho \Phi}{M_{nucl.}} \right) \frac{m_\rho^2}{g_\rho^2} R^2 \\ & - \frac{1}{2} \frac{m_\delta^2}{g_\delta^2} D^2. \end{aligned} \quad (2)$$

The energy density of the nucleon in the meson medium is  $E_i^*(k_i) = \sqrt{k_i^2 + M_i^{*\ 2}}$ , where  $M_i^*$  is the effective mass calculated in Eq. (6) and  $k_i$  is the momentum of the nucleon, where  $i = p, n$ . The  $\rho_b$  and  $\rho_3$  in Eq. (1) are the baryonic and iso-vector density respectively.  $\gamma$  is the spin degeneracy factor which is equal to 2 for individual nucleons.  $M_{nucl.}$  is the mass of the nucleon which is 939 MeV.

## 2.2 Interaction between nucleons and DM candidates in NM

It is a well known fact that the NS is rotating along with the galaxy. The DM halo in the Universe is also rotating so that the DM particles accreted mostly in the NS core due to its very high gravitational field and high baryon density (Goldman & Nussinov 1989; Kouvaris 2008; Xiang et al. 2014; Das et al. 2019). When DM particles interact with nucleons, it loses energy and helps in the cooling of the NS (Bhat & Paul 2019). The cooling of the NS are detailed in these Refs. (Gnedin et al. 2001; Page et al. 2004; Yakovlev & Pethick 2004; Yakovlev et al. 2005, 2010). The amount of DM inside the NS depends on

the evolution time of the NS in the Universe. In this context, we consider the Neutralino (Martin 1998; Panotopoulos & Lopes 2017) as a fermionic DM candidate which interact with nucleon via SM Higgs. The interaction Lagrangian of DM and nucleons is given as (Panotopoulos & Lopes 2017; Quddus et al. 2019; Das et al. 2019)

$$\begin{aligned} \mathcal{L} = & \mathcal{L}_{nucl.} + \bar{\chi} [i\gamma^\mu \partial_\mu - M_\chi + yh] \chi + \frac{1}{2} \partial_\mu h \partial^\mu h \\ & - \frac{1}{2} M_h^2 h^2 + f \frac{M_{nucl.}}{v} \bar{\varphi} h \varphi, \end{aligned} \quad (3)$$

where  $\mathcal{L}_{nucl.}$  is the nucleon-mesons Lagrangian and  $\varphi$  and  $\chi$  are the nucleonic and DM wave functions respectively. We take the mass of Neutralino ( $M_\chi$ ) is 200 GeV, and the coupling constants between DM and SM Higgs is  $y$ , which can be found in the large Higgs mixing angle limit. Since the Neutralino is the super symmetric particle, it has the various gauge coupling constants in the electroweak sector of the standard model (Martin 1998). So depending on the different parameters, the values of  $y$  is in the range 0.001 – 0.1. Thus we take the value of  $y = 0.07$  in our calculations. The Higgs field directly couples to the nucleons with Yukawa interaction  $f \frac{M_{nucl.}}{v}$ , where  $f$  is proton-Higgs form factor. The detailed analytical expression for  $f$  can be found in (Cline et al. 2013). In lattice calculations (Alarcón et al. 2012; Young 2012), we can consider the value of  $f = 0.35$ , which is agreement with (Cline et al. 2013). The Higgs mass is  $M_h = 125$  GeV. The vacuum expectation value ( $v$ ) of Higgs is 246 GeV. From the Lagrangian in Eq. (3), we get the total energy density ( $\mathcal{E}$ ) and pressure ( $P$ ) for NM with DM given as (Panotopoulos & Lopes 2017; Das et al. 2019; Quddus et al. 2019)

$$\begin{aligned} \mathcal{E} = & \mathcal{E}_{nucl.} + \frac{2}{(2\pi)^3} \int_0^{k_f^{DM}} d^3k \sqrt{k^2 + (M_\chi^*)^2} \\ & + \frac{1}{2} M_h^2 h_0^2, \end{aligned} \quad (4)$$

$$\begin{aligned} P = & P_{nucl.} + \frac{2}{3(2\pi)^3} \int_0^{k_f^{DM}} \frac{d^3k k^2}{\sqrt{k^2 + (M_\chi^*)^2}} \\ & - \frac{1}{2} M_h^2 h_0^2, \end{aligned} \quad (5)$$

where  $k_f^{DM}$  is the DM Fermi momentum. We consider the baryon density inside NS is 1000 times larger than the DM density, this imply that  $M_\chi/M=1/6$  (Panotopoulos & Lopes 2017; Das et al. 2019), where  $M$  is the mass of the NS. One can get  $k_f^{DM}$  is  $\sim 0.03$  GeV (Das et al. 2019). So that we vary  $k_f^{DM}$  from 0 – 0.06 GeV. The effective masses of nucleon and DM are given as

$$\begin{aligned} M_i^* &= M_{nucl.} + g_\sigma \sigma_0 \mp g_\delta \delta_0 - \frac{f M_{nucl.}}{v} h_0, \\ M_\chi^* &= M_\chi - y h_0, \end{aligned} \quad (6)$$

where the  $\sigma_0, \delta_0$  and  $h_0$  are the meson field equations of  $\sigma, \delta$  and Higgs respectively and these are obtained by applying mean field approximations, which are given in Ref. (Das et al. 2019). The DM density  $\rho_\chi$  is

$$\rho_\chi = \frac{\gamma}{(2\pi)^3} \int_0^{k_f^{DM}} \frac{M_\chi^*}{\sqrt{M_\chi^{*\ 2} + k^2}} d^3k, \quad (7)$$

## 2.3 NM Parameters

The calculations of NM properties need the energy density and pressure as a function of baryonic density. The energy density  $\mathcal{E}$  can

be expanded in a Taylor series in terms of  $\alpha$  (Horowitz et al. 2014; Baldo & Burgio 2016; Kumar et al. 2018).

$$\mathcal{E}(\rho, \alpha) = \mathcal{E}(\rho, \alpha = 0) + S(\rho)\alpha^2 + \mathcal{O}(\alpha^4), \quad (8)$$

where  $\mathcal{E}(\rho, \alpha = 0)$  is the energy of symmetric NM,  $\rho$  is the baryonic density and  $S(\rho)$  is the symmetry energy, which is defined as

$$S(\rho) = \frac{1}{2} \left( \frac{\partial^2 \mathcal{E}}{\partial \alpha^2} \right)_{\alpha=0} \quad (9)$$

The symmetry energy is also written as the energy difference between pure neutron matter (PNM) and symmetric NM (SNM) or vice-versa through parabolic approximation, i.e.

$$S(\rho) = \frac{\mathcal{E}(\rho, \alpha = 1) - \mathcal{E}(\rho, \alpha = 0)}{\rho}. \quad (10)$$

Although, the value of symmetry energy is fairly known at the saturation density ( $\rho_0$ ), its density dependence nature is not well known. The behavior of  $S(\rho)$  in high density, both qualitatively and quantitatively shows a great diversion depending on the model used (Li et al. 2019). Similar to the BE/A, the  $S(\rho)$  can also be expressed in a leptodermous expansion near the NM saturation density. The analytical expression of density dependence symmetry energy is written as (Matsui 1981; Kubis & Kutschera 1997; Del Estal et al. 2001; Chen & Piekarewicz 2014; Kumar et al. 2018):

$$S(\rho) = J + L\zeta + \frac{1}{2}K_{sym}\zeta^2 + \frac{1}{6}Q_{sym}\zeta^3 + \mathcal{O}(\zeta^4), \quad (11)$$

where  $\zeta = \frac{\rho - \rho_0}{3\rho_0}$ ,  $J = S(\rho_0)$  and the parameters like slope ( $L$ ), curvature ( $K_{sym}$ ) and skewness ( $Q_{sym}$ ) of  $S(\rho)$  are

$$L = 3\rho \frac{\partial S(\rho)}{\partial \rho}, \quad (12)$$

$$K_{sym} = 9\rho^2 \frac{\partial^2 S(\rho)}{\partial \rho^2}, \quad (13)$$

$$Q_{sym} = 27\rho^3 \frac{\partial^3 S(\rho)}{\partial \rho^3}. \quad (14)$$

The NM incompressibility ( $K$ ) is defined as (Chen & Piekarewicz 2014)

$$K = 9\rho^2 \frac{\partial}{\partial \rho} \left( \frac{P}{\rho^2} \right). \quad (15)$$

To estimate both symmetry energy and its slope parameters at saturation density  $\rho_0$ , we use Eq. (10). Since the parameters  $J$  and  $L$  play important roles like, formation of clusters in finite nuclei and normal star, dynamic of heavy-ion collisions and cooling process of newly born NS. These parameters are also crucial for the study of phase transition (finite/infinite nuclear systems). Different approaches are available for the calculation of  $J$  and  $L$  including their correlations (Centelles et al. 2009; Xu et al. 2010; Fattoyev et al. 2012; Steiner & Gandolfi 2012; Newton et al. 2012; Dutra et al. 2012; Singh et al. 2013).

## 2.4 The EoS of NS

In this section, we describe the NS EoS within a medium of nucleons, electrons and muons. In the NS, the neutron decays to proton, electron and anti-neutrino (Glendenning 1997; Quddus et al. 2019; Bhat & Paul 2019). There is also inverse  $\beta$ -decay to maintain the beta

equilibrium and charge neutrality condition. This can be expressed as (Glendenning 1997)

$$\begin{aligned} n &\rightarrow p + e^- + \bar{\nu}, \\ p + e^- &\rightarrow n + \nu. \end{aligned} \quad (16)$$

The stability of NSs is followed by  $\beta$ -equilibrium and charge-neutrality conditions as follow as

$$\begin{aligned} \mu_n &= \mu_p + \mu_e, \\ \mu_e &= \mu_\mu, \end{aligned} \quad (17)$$

where,  $\mu_n$ ,  $\mu_p$ ,  $\mu_e$ , and  $\mu_\mu$  are the chemical potentials of neutrons, protons, electrons, and muons, respectively, and the charge neutrality conditions is

$$\rho_p = \rho_e + \rho_\mu. \quad (18)$$

The chemical potentials  $\mu_n$ ,  $\mu_p$ ,  $\mu_e$ , and  $\mu_\mu$  are given by

$$\mu_n = g_\omega \omega_0 + g_\rho \rho_0 + \sqrt{k_n^2 + (M_n^*)^2}, \quad (19)$$

$$\mu_p = g_\omega \omega_0 - g_\rho \rho_0 + \sqrt{k_p^2 + (M_p^*)^2}, \quad (20)$$

$$\mu_e = \sqrt{k_e^2 + m_e^2}, \quad (21)$$

$$\mu_\mu = \sqrt{k_\mu^2 + m_\mu^2}, \quad (22)$$

where  $M_n^*$  and  $M_p^*$  is the effective masses of neutron and proton respectively calculated in Eq. (6). To find the particle fraction, we solve Eq. (17) and (18) followed by Eqs. (19–22) in a self-consistent way for a given baryon density. The total energy density and pressure of NS are given by,

$$\begin{aligned} \mathcal{E}_{NS} &= \mathcal{E} + \mathcal{E}_l, \\ \text{and } P_{NS} &= P + P_l, \end{aligned} \quad (23)$$

where,

$$\mathcal{E}_l = \sum_{l=e,\mu} \frac{2}{(2\pi)^3} \int_0^{k_l} d^3k \sqrt{k^2 + m_l^2}, \quad (24)$$

and

$$P_l = \sum_{l=e,\mu} \frac{2}{3(2\pi)^3} \int_0^{k_l} \frac{d^3k k^2}{\sqrt{k^2 + m_l^2}}. \quad (25)$$

Where  $\mathcal{E}_l$ ,  $P_l$  and  $k_l$  are the energy density, pressure and Fermi momentum for leptons respectively. The Eq. (23) gives the total energy, pressure and number density of the NS.

## 2.5 Observables of the NS

In the Sec. 1, we have already mention that NS is very complex structure and therefore the detailed study require both theories of GR and dense matter. i.e NS forms a link between two fundamental theory in the modern physics and this connection already given by Einstein's field equation (Einstein 1916)

$$G^{\mu\nu} = R^{\mu\nu} - \frac{1}{2}g^{\mu\nu}R = 8\pi T^{\mu\nu}, \quad (26)$$

where  $G^{\mu\nu}$ ,  $R^{\mu\nu}$ ,  $g^{\mu\nu}$  and  $R$  are the Einstein tensor, Ricci tensor, metric tensor and Ricci scalar respectively. The  $T^{\mu\nu}$  is the energy-momentum tensor for perfect fluid is given as (Glendenning 1997; Krastev et al. 2008)

$$T^{\mu\nu} = (\mathcal{E}_{NS} + P_{NS})u^\mu u^\nu + P g^{\mu\nu}, \quad (27)$$

where  $\mathcal{E}_{NS}$  and  $P_{NS}$  are the energy density and pressure of the NS.  $u^\mu$  is the 4-velocity satisfying,  $u^\mu u_\mu = -1$ . The  $T^{\mu\nu}$  directly depends on the EoS of the stellar matter in the form of  $P_{NS}(\mathcal{E}_{NS})$ . To solve the Einstein's Eq. 26, First, we have to solve the short-range nuclear forces of many-body nuclear physics in a local inertial frame in which space-time is flat. Second, the long range force of the gravitational field which describe the curvature of space-time created by the massive objects (Krastev et al. 2008). We calculate the many-body theory using RMF formalism in Sub-Sec. 2.1. But in this present Sub-Sec. we calculate the different observables like  $M$ ,  $R$  and  $I$  etc. for the NS. In our whole calculations we use  $G = c = 1$ .

In case of static, spherically symmetric stars the metric is in the form of

$$ds^2 = -e^{2\nu(r)} dt^2 + e^{2\lambda(r)} dr^2 + r^2 d\theta^2 + r^2 \sin^2 \theta d\phi^2, \quad (28)$$

where  $r$ ,  $\theta$  and  $\phi$  are the spherical co-ordinates.  $\nu(r)$ ,  $\lambda(r)$  are the metric potential are given as (Krastev et al. 2008)

$$e^{2\lambda(r)} = [1 - \gamma(r)]^{-1}, \quad (29)$$

$$e^{2\nu(r)} = e^{-2\lambda(r)} = [1 - \gamma(r)], \quad r > R_{star} \quad (30)$$

with

$$\gamma(r) = \begin{cases} \frac{2m(r)}{r}, & \text{if } r < R_{star} \\ \frac{2M}{r}, & \text{if } r > R_{star} \end{cases} \quad (31)$$

For static star, the Einstein's Eq. 26 reduces to

$$\frac{dP_{NS}(r)}{dr} = -\frac{[P_{NS}(r) + \mathcal{E}_{NS}(r)][m(r) + 4\pi r^3 P_{NS}(r)]}{r[r - 2m(r)]}, \quad (32)$$

and

$$\frac{dm(r)}{dr} = 4\pi r^2 \mathcal{E}_{NS}(r), \quad (33)$$

where  $\mathcal{E}_{NS}(r)$  and  $P_{NS}(r)$  are the total energy density and pressure appearing in Eq. (23) under the  $\beta$ -equilibrium condition.  $m(r)$  is the gravitational mass, and  $r$  is the radial parameter. These two coupled equations are solved to get the  $M$  and  $R$  of the SNS at certain central density.

The metric of RNS in equilibrium is described by a stationary and axisymmetric metric of the form (Stergioulas 2003)

$$ds^2 = -e^{2\nu} dt^2 + e^{2\psi} (d\phi - \omega dt)^2 + e^{2\alpha} (r^2 d\theta^2 + d\phi^2), \quad (34)$$

where  $\nu$ ,  $\psi$ ,  $\omega$  and  $\alpha$  are metric functions which depend on  $r$  and  $\theta$  only. The energy-momentum tensor same as in Eq. 27, but the 4-velocity is changed as follow as

$$u^\mu = \frac{e^\mu}{\sqrt{1 - \nu^2}} (t^\mu + \Omega \phi^\mu), \quad (35)$$

and the spatial velocity,  $v = (\Omega - \omega)e^{\psi - \nu}$ , where  $\Omega$  is the angular velocity of the star.  $t^\mu$  and  $\phi^\mu$  are two killing vectors in the space-time associated with time and transnational symmetries.

Many people have calculated the moment of inertia of the NS

**Table 1.** The 3-parameter sets NL3 (Lalazissis et al. 1997), G3 (Kumar et al. 2017) and IOPB-I (Kumar et al. 2018) are listed. All the coupling constants are dimensionless.

Parameter	NL3	G3	IOPB-I
$m_\sigma/M_{nucl.}$	0.541	0.559	0.533
$m_\omega/M_{nucl.}$	0.833	0.832	0.833
$m_\rho/M_{nucl.}$	0.812	0.820	0.812
$m_\delta/M_{nucl.}$	0.0	1.043	0.0
$g_\sigma/4\pi$	0.813	0.782	0.827
$g_\omega/4\pi$	1.024	0.923	1.062
$g_\rho/4\pi$	0.712	0.962	0.885
$g_\delta/4\pi$	0.0	0.160	0.0
$k_3$	1.465	2.606	1.496
$k_4$	-5.688	1.694	-2.932
$\zeta_0$	0.0	1.010	3.103
$\eta_1$	0.0	0.424	0.0
$\eta_2$	0.0	0.114	0.0
$\eta_\rho$	0.0	0.645	0.0
$\Lambda_\omega$	0.0	0.038	0.024

(Stergioulas 2003; Jha et al. 2008; Sharma & Jha 2009; Friedman & Stergioulas 2013; Paschalidis & Stergioulas 2017; Quddus et al. 2019; Koliogiannis & Moustakidis 2020). The simple expression is  $I = J/\Omega$ , where  $J$  is angular momentum and  $\Omega$  is the angular velocity of the NS. The expression of  $I$  of uniformly rotating NS with angular frequency  $\omega$  is given as (Lattimer & Prakash 2000; Worley et al. 2008)

$$I \approx \frac{8\pi}{3} \int_0^R (\mathcal{E}_{NS} + P_{NS}) e^{-\phi(r)} \left[1 - \frac{2m(r)}{r}\right]^{-1} \frac{\bar{\omega}}{\Omega} r^4 dr, \quad (36)$$

where the  $\bar{\omega}$  is the dragging angular velocity for a uniformly rotating star. The  $\bar{\omega}$  satisfying the boundary conditions are

$$\bar{\omega}(r=R) = 1 - \frac{2I}{R^3}, \quad \left. \frac{d\bar{\omega}}{dr} \right|_{r=0} = 0. \quad (37)$$

The Keplerian frequency of the NS also calculated in these Refs. (Komatsu et al. 1989a,b; Stergioulas 2003; Dhiman et al. 2007; Jha et al. 2008; Krastev et al. 2008; Worley et al. 2008; Haensel et al. 2009; Sharma & Jha 2009; Koliogiannis & Moustakidis 2020) and the expression is given as

$$\nu_k(M) \approx \chi \left(\frac{M}{M_\odot}\right)^{1/2} \left(\frac{R}{10 \text{ km}}\right)^{-3/2}, \quad (38)$$

where  $M$  and  $R$  are the gravitational mass and radius of the RNS respectively. The value of  $\chi$  is calculated from the fitting or empirically (Lattimer & Prakash 2004; Haensel et al. 2009). In Ref. (Haensel et al. 2009), they have found the value of  $\chi = 1.08$  kHz empirically. For rotating NS, we calculate the  $M$ ,  $R$ ,  $I$  and Keplerian frequency ( $\nu_K$ ) using public-domain program, RNS code written by the Stergioulas (Stergioulas & Morsink 1999).

### 3 RESULTS AND DISCUSSIONS

In this section, we present the calculated results for BE/A,  $K$ ,  $S$  and its derivatives for NM varying the  $k_f^{DM}$  at different  $\alpha$ . We extend the calculations to NSs and find the  $M$ ,  $R$  and  $I$ .

#### 3.1 NM Properties

The  $\mathcal{E}$  and  $P$  are obtained using RMF approaches with DM (Panotopoulos & Lopes 2017; Quddus et al. 2019; Das et al. 2019) in Eqs.

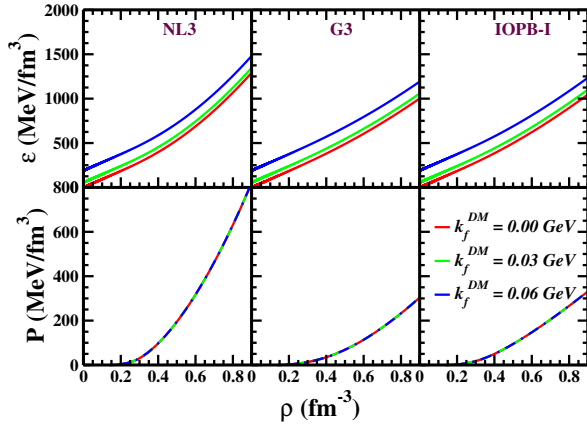


**Figure 1.** (colour online) The energy density (Eq. 4) and pressure (Eq. 5) for SNM with baryon density at  $k_f^{DM} = 0.0, 0.03$  and  $0.06$  GeV.

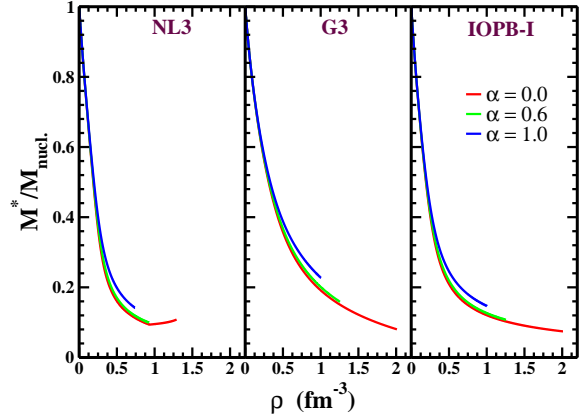


**Figure 3.** (colour online) The variation of effective mass in Eq. (6) for different  $\alpha$  with baryon density with  $k_f^{DM} = 0.06$  GeV.

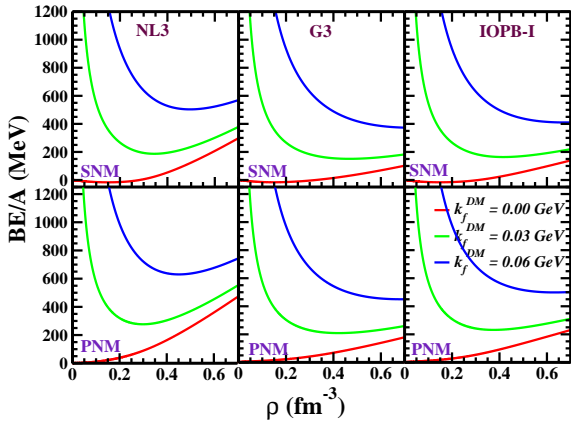


**Figure 2.** (color online) The BE/A of NM in the presence of DM at  $k_f^{DM} = 0.0, 0.03$  and  $0.06$  GeV.

4 and 5. The  $\mathcal{E}$  and  $P$  as a function of baryon density  $\rho$  are shown in Fig. 1. The RMF forces NL3 (Lalazissis et al. 1997), G3 (Kumar et al. 2017) and IOPB-I (Kumar et al. 2018) are given in Table 1. Since, the  $k_f^{DM}$  is not yet settled, we change its values for  $k_f^{DM} = 0.0, 0.03$  and  $0.06$  GeV and note down the variations as a function of  $\rho$  in Fig. 1. We notice that the value of  $\mathcal{E}$  changes significantly without affecting the  $P$  (see Fig. 1). NL3 gives the stiffest EoS as compare to IOPB-I and G3 for the SNM case. Here also, G3 predicts the softest EoS, which is shown in the Fig. 1. Thus, the qualitative nature of the EoS is similar with and without the presence of DM as far as stiffness or softness is concerned. The BE/A is defined as  $\frac{\mathcal{E}}{\rho} - M_{nucl.}$ , where the  $\mathcal{E}$  is the total energy density in Eq. (4) and  $\rho$  is the baryon density. The BE/A as a function of  $\rho$  at different  $k_f^{DM}$  is shown in Fig. 2 for both SNM and PNM. Here the effect of DM on BE/A is significant with respect to  $k_f^{DM}$  for both SNM and PNM.

The NS is mostly made of neutrons with a small fraction of protons, electrons and muons in the charge-neutral and  $\beta$ -equilibrium system. Thus to get an idea about the NM parameters, we check the variation of the effective mass ( $M^*$ ) with different  $\alpha$ . Here it is imperative to mention that  $k_f^{DM} = 0$  GeV means  $\rho_\chi$  is zero, but the effect on  $M^*$

is very less due to non-zero Higgs-nucleon Yukawa coupling in Eq. (6). The contribution of Higgs field is very small  $O(10^{-6} - 10^{-8})$  even after varying  $k_f^{DM}$  to its maximum value. So that we plot the effective mass to mass ratio of the nucleon ( $M^*/M_{nucl.}$ ) as a function of  $\rho$  for different  $\alpha$ , which is shown in Fig. 3. In the presence of DM, the  $M^*/M_{nucl.}$  decreases with baryon density  $\rho$ , similar to the normal nuclear medium. As far as the neutron to proton ratio ( $N/Z$ ) increases, the  $M^*/M_{nucl.}$  value goes on increasing mostly in the high-density region. However, there is practically no effect of  $\alpha$  in the low-density region of the NM system.

Another important NM parameter is  $K$ . This value tells us how much one can compress the NM system. It is a standard quantity at the saturation point. However, an astronomical object like the NS, its density varies from the centre of the star to the crust with a variation of  $\rho$  from  $\rho = 10\rho_0$  to  $0.1\rho_0$  (Lattimer & Prakash 2004). Thus, to achieve better knowledge on the compression mode or monopole vibration mode, we have to calculate the  $K$  for all the density range of NM with different  $\alpha$  including 0 and 1. Since we see the earlier case, DM does not affect on the pressure of either SNM or PNM also in NS (in sec. 3.2), so DM doesn't affect the  $K$  of NM. The variation of  $K$  with baryon density for different  $\alpha$  displayed in Fig. 4. One can see in Table 2, for SNM system the incompressibility at saturation  $K_\infty$  are 271.38, 243.96 and 222.65 MeV for NL3, G3 and IOPB-I respectively. It is worthy of mentioning that the DM does not affect on the incompressibility. That means, the  $K$  values remain unaffected with the variation of  $k_f^{DM}$ . On the other hand, substantial variation is seen with the different  $\alpha$ . We found that the value of  $K$  increases initially up to a maximum and then gradually decreases, as shown in Fig. 4. The calculations also show that with increasing  $\alpha$ , the incompressibility decreases irrespective of the parameter sets. The values of  $K$  for G3 and IOPB-I parameter sets lie in the region (except for NL3) given by the experimental value in Table 2. Since the NL3 gives very stiff EOS so that it's all NM parameters like  $K$ ,  $J$ ,  $L$  etc. provide very large values and do not lie the region given in Table 2.

The recent gravitational wave observation from the merger of two NSs, the GW170817 (Abbott et al. 2017, 2018), constraints the upper limit on the tidal deformability  $\Lambda$  and predicts a small

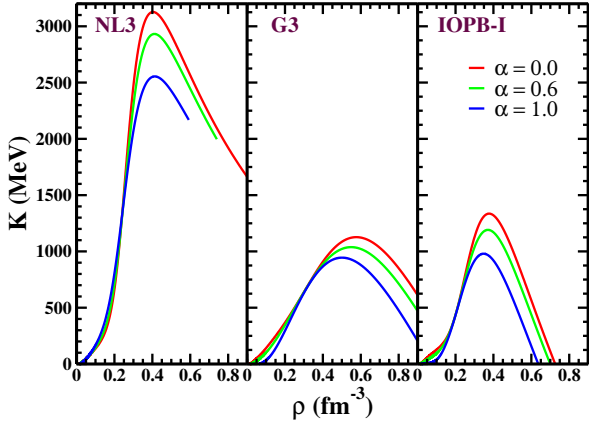


**Figure 4.** (colour online) The variation of incompressibility  $K$  with different  $\alpha$  as a function of baryon density  $\rho$  with  $k_f^{DM} = 0.06 \text{ GeV}$ .

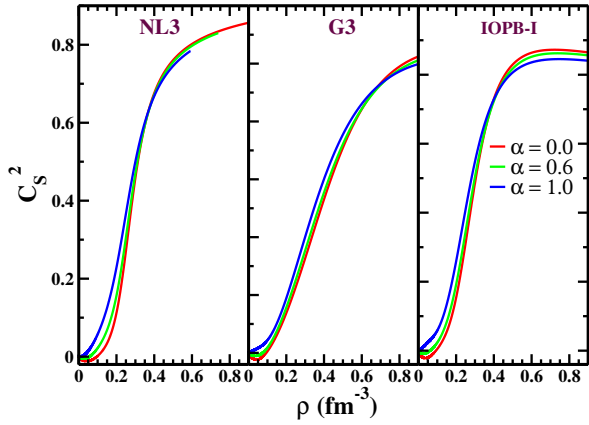


**Figure 5.** (colour online) The variation of speed of the sound with baryon density for NL3, G3 and IOPB-I parameterizations at different  $\alpha$  with  $k_f^{DM} = 0.06 \text{ GeV}$ .

radius. Also, the recent discovery of the three highly massive stars  $\sim 2 M_\odot$  (Antoniadis et al. 2013; Fonseca et al. 2016; Cromartie et al. 2019) predicts that the pressure in the inner core of the star is large, where the typical baryon number density quite high  $\rho > 3\rho_0$  in this region. The pressure in the outer core of the massive NS is considered to be small in the density range 1 to  $3\rho_0$  (McLerran & Reddy 2019). Combining these observations of large masses and the smaller radii of the massive NSs, one can infer that the causality (Rhoades & Ruffini 1974; Bedaque & Steiner 2015; Kojo et al. 2015; Moustakidis et al. 2017; McLerran & Reddy 2019) of the NM inside the inner core of the NS can violate (McLerran & Reddy 2019). It is conjectured that the speed of the sound  $C_s \leq c/\sqrt{3}$ , where  $C_s^2 = \frac{\partial P}{\partial \epsilon}$  with  $C_s$  and  $c$  are the speed of the sound and light, respectively. To see the causality condition for the NM case with an admixture of DM, we plot  $C_s^2$  as a function of baryon number density  $\rho$  in Fig. 5 at different  $\alpha$  for NL3, G3 and IOPB-I parameter sets. We find that the  $C_s^2$  increases approximately up to  $0.8 \text{ fm}^{-3}$ , then it is constant for high density regions. It is clear from the values of  $C_s^2$  that the causality remains intact for a wide range of density for all three parameter sets, as shown in Fig. 5.

The symmetry energy  $S$  and its coefficients  $L$ ,  $K_{sym}$  and  $Q_{sym}$  are defined in Eqs. (12 – 14), play a crucial role in the EoS for symmetric and asymmetric NM. As we have mentioned earlier,

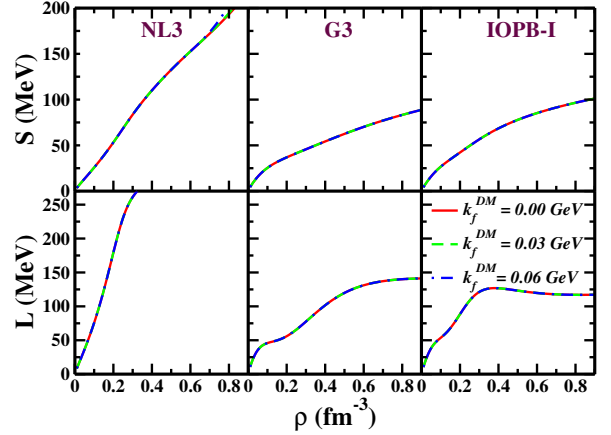


**Figure 6.** (colour online) The symmetry energy  $S$  and its slope parameter  $L$  are plotted with the varying  $k_f^{DM}$  as a function of with  $\rho$ . We found almost the same results ( Table 2 ) with and without DM for all the three-parameter sets.

these parameters are important quantities to determine the nature of the EoS. Just after the supernova explosion, its remnants, which lead towards the formation of a NS, is in a high temperature ( $\sim 200 \text{ MeV}$ ) state (Gnedin et al. 2001; Page et al. 2004; Yakovlev & Pethick 2004; Yakovlev et al. 2005, 2010). Soon after the formation of the NS, it starts cooling via the direct urca processes to attain the stable charge neutrality and  $\beta$ -equilibrium condition. The dynamical process of NS cooling is affected heavily by these NM parameters. Thus, it is very much intuitive to study these parameters in more rigorously. The  $S$  and its  $L$ -coefficient for the whole density range for all three parameter sets NL3, G3 and IOPB-I with different  $k_f^{DM}$  are displayed in Fig. 6. The effect of DM on  $J$  and  $L$  is very small, and it is difficult to notice in the figure. To have the knowledge, we summarised the results at the saturation point in Table 2. For example, with NL3 set,  $S(\rho_0) = J = 37.43 \text{ MeV}$  for PNM and it increases to a value  $J = 38.36 \text{ MeV}$  with DM. Similarly,  $L = 118.65 \text{ MeV}$  for without DM,  $L = 121.44$  and  $121.45 \text{ MeV}$  in the presence of DM for various DM momentum  $k_f^{DM}$ . For other sets, one can see the variation in Table 2. This is due to the fact that the effect of DM does not change NM asymmetry to a significant extent. A careful inspection of Fig. 6 and Table 2, it is clear that  $S$  and  $L$  are force-dependent. It is maximum for NL3 and minimum for G3 sets. The experimental value of  $J$  and  $L$  is given in the Table 2 at  $\rho_0$  is in between  $30.2 - 33.7 \text{ MeV}$  and  $35.0 - 70.0 \text{ MeV}$  respectively. With the addition of DM, the values of  $J$  and  $L$  lie (except for NL3) in this region as given in the Table 2.

The other higher-order derivatives of symmetry energy like  $K_{sym}$  and  $Q_{sym}$  are also calculated in this section. The results are displayed in Fig. 7 and their numerical values are tabulated in Table 2. The  $K_{sym}$  is a parameter, which tells a lot not only about the surface properties of the astrophysical object (such as NS and white dwarf), but also the surface properties of finite nuclei. The whole density range of  $K_{sym}$  and  $Q_{sym}$  for G3 and IOPB-I sets are shown. The  $K_{sym}$  affected marginally, but the parameter  $Q_{sym}$  influenced significantly by DM (see Table 2) for these values at saturation. At low density,  $K_{sym}$  initially decreases slightly, then it increases up to  $\rho$  ( $\sim 0.2 \text{ fm}^{-3}$ ) and after that decreases the value almost like an exponential function. Recently the value of  $K_{sym}$  is calculated by Zimmerman et al. (Zimmerman et al. 2020) with the help of NICER (Miller et al. 2019; Riley et al. 2019; Bogdanov et al. 2019; Bilous et al. 2019;

**Table 2.** The nuclear matter properties such as BE/A, symmetry energy and its derivatives etc. are given at saturation density for three-parameters sets with  $k_f^{DM} = 0$  GeV (without DM), 0.03 GeV and 0.06 GeV respectively for SNM. Similarly the effective mass ( $M^*/M_{nucl}$ ), incompressibility ( $K$ ) varying with  $\alpha = 0, 0.6, 1.0$  at  $\rho_0$  (not in the variations of  $k_f^{DM}$ ) in last three-rows. The empirical/expt. value for  $\rho_0$ , BE/A,  $J$ ,  $L$ ,  $K_{sym}$  and  $K$  are also given at saturation density.

Parameters	NL3			G3			IOPB-I			Empirical/Expt. value
	0.0	0.03	0.06	0.0	0.03	0.06	0.0	0.03	0.06	
$\rho_0$ ( $\text{fm}^{-3}$ )	0.148	0.148	0.148	0.148	0.148	0.148	0.149	0.149	0.149	0.148 – 0.185 (Bethe 1971)
BE/A (MeV)	-16.35	143.95	1266.11	-16.02	143.28	1266.44	-16.10	143.09	1257.51	-15 – -17 MeV (Bethe 1971)
$J$ (MeV)	37.43	38.36	38.36	31.84	31.62	31.62	33.30	34.45	34.45	30.20 – 33.70 MeV (Danielewicz & Lee 2014)
$L$ (MeV)	118.65	121.44	121.45	49.31	49.64	49.64	63.58	67.16	67.67	35.00 – 70.00 MeV (Danielewicz & Lee 2014)
$K_{sym}$ (MeV)	101.34	101.05	100.32	-106.07	-110.38	-111.10	-37.09	-45.94	-46.67	-174 – -31 MeV (Zimmerman et al. 2020)
$Q_{sym}$ (MeV)	177.90	115.56	531.30	915.47	929.67	1345.40	868.45	927.84	1343.58	—————
$\alpha =$	0	0.6	1.0	0	0.6	1.0	0	0.6	1.0	
$M^*/M_{nucl}$ .	0.595	0.596	0.606	0.699	0.700	0.704	0.593	0.599	0.604	—————
$K$ (MeV)	271.38	312.45	372.13	243.96	206.88	133.04	222.65	204.00	176.28	220 – 260 MeV (Stone et al. 2014)

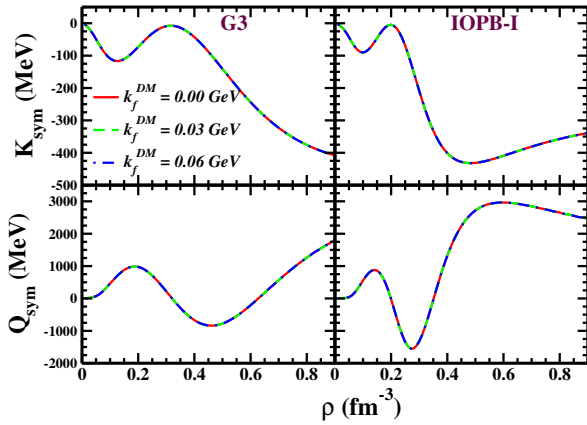


**Figure 7.** (colour online) The variation of  $K_{sym}$  and  $Q_{sym}$  with baryon density is plotted for G3 and IOPB-I at different  $k_f^{DM}$ . The  $K_{sym}$  and  $Q_{sym}$  are opposite to each other both for G3 and IOPB-I.

Raaijmakers et al. 2019; Guillot et al. 2019) and GW170817 data and its values lies in the range -174 to -31 MeV as given in Table 2. Our  $K_{sym}$  values lie in this region at the saturation density.

### 3.2 Neutron Star Matter

As an application of our mixed EoS, i.e. DM and hadron matter, we used the EoS to calculate the M, R and I of RNS. For this, we constructed the star EoS maintaining the charge neutrality and  $\beta$ -equilibrium condition varying the DM momentum  $k_f^{DM}$ . The EoS for NL3, G3 and IOPB-I at  $k_f^{DM} = 0.0, 0.03$  and  $0.06$  GeV are shown in Fig. 8. As we have mentioned earlier in the PNM and SNM, the EoS is very sensitive to  $k_f^{DM}$ , here also the energy density  $\mathcal{E}$  is equally sensitive to the DM. We find softer EoS as in (Li et al. 2012; Panotopoulos & Lopes 2017; Bhat & Paul 2019; Das et al. 2019; Quddus et al. 2019) with  $k_f^{DM}$ . Similar to the SNM and

PNM, NL3 predicts the stiffest and G3 the softest EoS for different  $k_f^{DM}$ . The calculations of  $M$ ,  $R$  and  $I$  of the SNS and RNS need the entire EoS of the NS. In crust region, which has very low density ( $< 5 \times 10^{14}$  g  $\text{cm}^{-3}$ ), the inter nucleon distances is higher than the core region of the NS and the clusterisation of the nucleon happens. In the core region, due to the high density the NS system behave like a incompressible fluid of the nucleons. For the core part, we use the RMF equation of state. In crust part, we use BPS (Baym et al. 1971) EoS. Construction of the BPS EoS is based on the minimisation of the Gibbs function and effects of the Coulomb lattice, which gives a suitable combination of the A and Z. Once we know the entire EoS, we can calculate the properties of the SNS solving TOV equations (Tolman 1939; Oppenheimer & Volkoff 1939) and RNS using RNS code (Stergioulas & Morsink 1999). The brief formalism for RNS can be found in Sub-Sec. 2.5.

Before calculating the  $M$  and  $R$ , we tested the causality condition (Rhoades & Ruffini 1974; Bedaque & Steiner 2015; Kojo et al. 2015; Moustakidis et al. 2017; McLerran & Reddy 2019) in the NS medium with an admixture of DM. We have seen that both in NM and NS matter case, the causality is not violated throughout the region, as shown in Fig. 5 and 9 respectively. The dashed horizontal line is the conjectured  $C_s^2 = 1/3$  value given in Fig. 9. The NL3 predicts the stiff rise in  $C_s^2$  as compared to G3 and IOPB-I. But in all the cases  $C_s^2$  is less than  $1/3$  for very low density region ( $\rho < 0.4$   $\text{fm}^{-3}$ ). As compared to the NM, the NS contains nucleons, electrons and muons, which is completely a different stable system survived by the balancing force due to the attractive gravitation and the repulsive degenerate neutrons also with short-range repulsive nuclear force.

Now, we calculate the M-R relations and  $I$  for G3 as a representative case. The M-R relation for different  $k_f^{DM}$  are shown in Fig. 10. The results from the precisely measured NSs masses, such as PSR J1614-2230 (Demorest et al. 2010) and PSR J0740+6620 (Cromartie et al. 2019) are shown in the horizontal lines in pink colours. These observations suggest that the maximum mass predicted by any the-



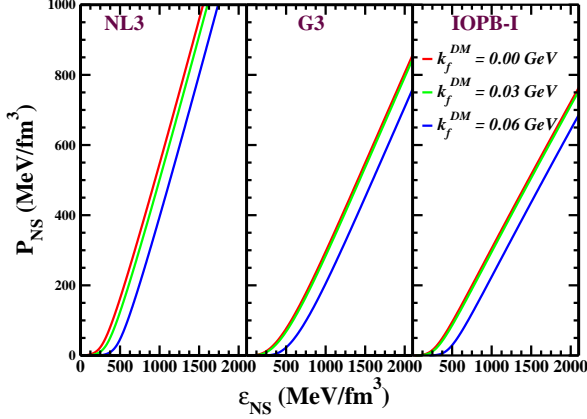


**Figure 8.** (colour online) The variation of energy density and pressure in Eq. (23) with different  $k_f^{DM}$ . We find NL3 is the stiffest and G3 is the softest.

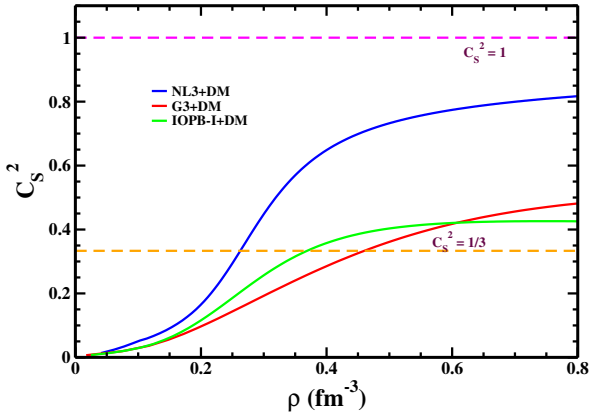


**Figure 9.** (colour online) The speed of the sound is plotted with the baryon density for 3-parameters sets with  $k_f^{DM} = 0.06$  GeV. The orange dashed line represents the conjecture ( $C_s^2 = 1/3$ ) and magenta dashed line represents the  $C_s^2$  is equal to  $c$ .

oretical model should reach the limit  $\sim 2.0 M_\odot$ , and this condition is satisfied in all of the EoSs, which are taken into consideration. We noticed that the increase in  $k_f^{DM}$ , higher the energy density at a given  $\rho$ , which yield the lower the maximum mass and radius of the SNS and RNS. For RNS case the maximum mass is increased by  $\sim 20\%$ , and radius increased by  $\sim 26\%$  for the given EoS, which is approximately equal to the increase in mass due to the rapid rotation of the NS (Stergioulas 2003; Worley et al. 2008).

Here, we examine the effect of Kepler frequency ( $\nu_K$ ) on the mass of the NS. In Fig. 10, the mass of the RNS is increased due to the rapid rotation of the NS due to its high  $\nu_K$ , i.e. the mass of NS directly depends on the  $\nu_K$ . Theoretical calculations allows the value of  $\nu_K$  is more than 2000 Hz (Koliogiannis & Moustakidis 2020), but till now two fastest pulsar was detected having frequency 716 Hz (Hessels et al. 2006) and 1122 Hz (Kaaret et al. 2007). From Fig. 11, one can conclude that the NS mass approximately more than  $1.7 M_\odot$  is rotated more than the fastest pulsar as of today. In our case, we find the  $\nu_K$ s are 1553, 1671 and 2079 Hz for the DM momentum 0, 0.03 and 0.06 GeV respectively at the maximum mass. The spherical NS is

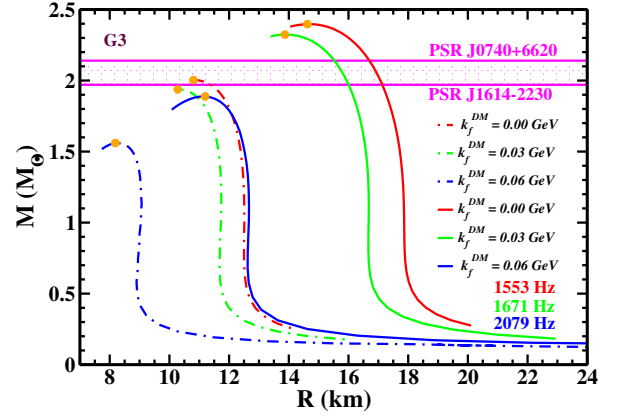


**Figure 10.** (colour online) The variation of mass with radius with different  $k_f^{DM}$  is shown. The orange colour dot shows the maximum mass of the corresponding  $k_f^{DM}$  for G3 parameter set. The dotted-dashed line represents for the SNS, and the bold line represents the RNS. The maximum rotational frequencies of NS also shown. The recent observational constraints on NS masses (Demorest et al. 2010; Cromartie et al. 2019) are also shown.

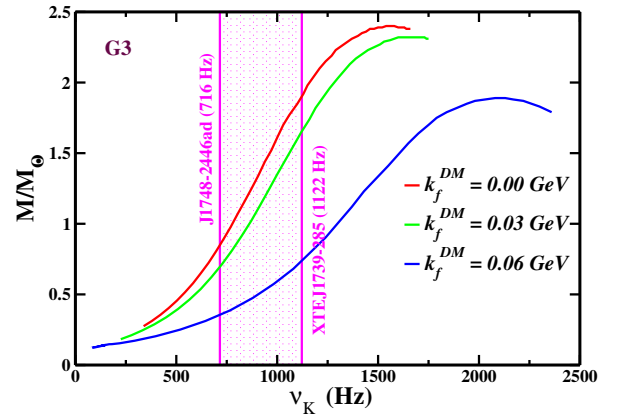


**Figure 11.** (colour online) The variation NS mass with Keplerian frequency  $\nu_K$  is shown for G3 parameter set. The two vertical magenta line represents the frequencies of the fastest NSs J1748-2446ad (Hessels et al. 2006) and XTE J1739-285 (Kaaret et al. 2007).

leading to deformed shape with the increasing of mass (or frequency)

A measurement of the  $I$  of PSR J0737-3039A is expected via optical observation of the orbital precision in the double pulsar system in the near future (Burgay et al. 2003). As the  $I$  depends on the internal structure of the NS, it's measurement will constrain the unknown EoS of supra-nuclear matter, which is believed to be universal for all NS (Landry & Kumar 2018; Kumar & Landry 2019). Here we show the variation of  $I$  with  $M$  in Fig. 12. The change of  $I$  with  $M$  is almost linear for different values of  $k_f^{DM}$  up to the maximum mass of the star. Then there is a drop of  $I$ , as shown in Fig. 12. Since the increase of DM momentum ( $k_f^{DM}$ ) leads to softer EoS, and hence the decrease of  $I$ . This is because  $I \sim MR^2$  is directly proportional to the mass and square of the radius of the rotating object. The moment of inertia is larger for the stiffer EoS as it predicts a larger radius and vice-versa.

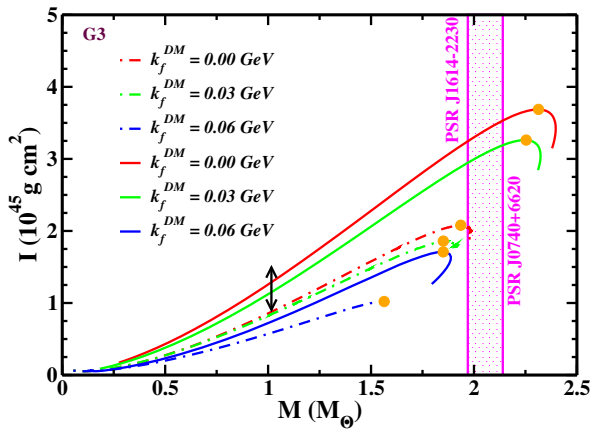


**Figure 12.** (colour online) The variation of  $I$  with the mass of NS for different  $k_f^{DM}$  using G3 parameter set. The orange colour dot shows the maximum mass of the corresponding  $k_f^{DM}$ . The dotted-dashed line represents for the SNS, and the bold line represents the RNS. The overlaid arrows represent the constraints on  $I$ , of PSR J0737-3039A set (Landry & Kumar 2018; Kumar & Landry 2019) from the analysis of GW170817 data (Abbott et al. 2017, 2018)

#### 4 SUMMARY AND CONCLUSIONS

In summary, we studied the effects of DM on the NM parameters, such as nuclear incompressibility ( $K$ ), symmetry energy ( $S$ ) and its higher-order derivatives like  $L$ -slope parameter,  $K_{sym}$ -isovector incompressibility and  $Q_{sym}$ -skewness parameter for different asymmetric. These are the significant quantities responsible for the behaviour of nuclear EoS. The EoS becomes softer or stiffer depending on the values of these parameters. We calculated these quantities taking different admixture of DM fraction in the NM with varying neutron-proton asymmetry. We take Neutralino as a DM candidate which is trapped inside the NS and its interaction to nucleons through SM Higgs via Yukawa potential. The RMF Lagrangian with NL3, G3 and IOPB-I forces are used to get the hadron EoS, and the DM part is added on top of it.

We find softer EoS with the increasing DM momentum, i.e. the energy density increases with  $k_f^{DM}$  without adding much to the pressure. The influence of DM on effective mass, symmetry energy,  $L$ -coefficient and  $K_{sym}$  are not much change with the variation of  $k_f^{DM}$  due to the small contributions of the Higgs field. However, some other derivatives of  $S$  ( $Q_{sym}$ ) and  $\mathcal{E}$  ( $K$ ) affected significantly by DM. These effects contribute to the mass, radius and moment of inertia of stellar object like a NS. Also, the variation of  $\mathcal{E}$ ,  $K$  and  $Q_{sym}$  due to DM not only affect the structure of NS but also significantly influence on the cooling effect of newly born NS after a supernova explosion. Thus, a detailed study of the temperature-dependent EoS is due, which will be published somewhere (Kumar et al. 2020).

To check the influence of DM on the accreting object, we constructed the NS EoS at various momenta of DM admixture. The mass, radius and the moment of inertia are evaluated for static as well as rotating cases using the TOV and RNS equations. The mass and radius are significantly reduced with the increase of DM momentum as we know that the stiffer EoS gives higher mass, radius and  $I$  of a RNS. The mass of the NS is significantly changed due to the rapid rotation of the NS. Quantitatively, the mass of NS approximately more than  $1.7 M_\odot$  are rotating having the frequency

more than the fastest pulsar ever detected.

#### ACKNOWLEDGEMENTS

H. C. Das would like to thank T. K. Jha for the fruitful discussion about the RNS code and Abhishek Roy for the necessary discussion on the DM. This work is supported in part by JSPS KAKENHI Grant No. 18H01209, and also S. K. Biswal and Ang Li are supported by the National Natural Science Foundation of China Grant No. 11873040.

#### REFERENCES

- Abbott B. P., et al., 2017, *Phys. Rev. Lett.*, 119, 161101  
 Abbott B. P., et al., 2018, *Phys. Rev. Lett.*, 121, 161101  
 Akmal A., Pandharipande V. R., Ravenhall D. G., 1998, *Phys. Rev. C*, 58, 1804  
 Alam N., Agrawal B. K., Fortin M., Pais H., Providência C., Raduta A. R., Sulaksono A., 2016, *Phys. Rev. C*, 94, 052801  
 Alarcón J. M., Camalich J. M., Oller J. A., 2012, *Phys. Rev. D*, 85, 051503  
 Alex Brown B., 1998, *Phys. Rev. C*, 58, 220  
 Ambartsumyan V. A., Saakyan G. S., 1960, *sovast*, 4, 187  
 Angle J., et al., 2008, *Phys. Rev. Lett.*, 101, 091301  
 Antoniadis J., et al., 2013, *Science*, 340, 1233232  
 Baldo M., Burgio G., 2016, *Progress in Particle and Nuclear Physics*, 91, 203–258  
 Baym G., Pethick C., Sutherland P., 1971, *APJ*, 170, 299  
 Bedaque P., Steiner A. W., 2015, *Phys. Rev. Lett.*, 114, 031103  
 Bernabei R., et al., 2008, *EPJ C*, 56, 333–355  
 Bernabei R., et al., 2010, *EPJ C*, 67, 39–49  
 Bernal N., Heikinheimo M., Tenkanen T., Tuominen K., Vaskonen V., 2017, *IJMP A*, 32, 1730023  
 Bertone G., Fairbairn M., 2008, *Phys. Rev. D*, 77, 043515  
 Bethe H. A., 1971, *Annual Review of Nuclear Science*, 21, 93  
 Bhat S. A., Paul A., 2019 ([arXiv:1905.12483](https://arxiv.org/abs/1905.12483))  
 Bhowmick B., Bhattacharya M., Bhattacharyya A., Gangopadhyay G., 2014, *Phys. Rev. C*, 89, 065806  
 Bhuyan M., 2018, *Physics of Atomic Nuclei*, 81, 15–23  
 Bhuyan M., Patra S. K., 2012, *Mod. Phys. Lett. A*, 27, 1250173  
 Bhuyan M., Carlson B. V., Patra S. K., Zhou S.-G., 2017, *IJMP E*, 26, 1750052  
 Bilous A. V., et al., 2019, *APJ*, 887, L23  
 Biswal S. K., 2019, *AIP Conf. Proceedings*, 2127, 020031  
 Biswal S., Kumar B., Patra S., 2016, *Int. J. Mod. Phys. E*, 25, 1650090  
 Biswal S. K., Patra S. K., Zhou S.-G., 2019, *APJ*, 885, 25  
 Bogdanov S., et al., 2019, *APJ*, 887, L26  
 Burgay M., et al., 2003, *Nature*, 426, 531  
 CDMS 2010, *Science*, 327, 1619–1621  
 Carson Z., Steiner A. W., Yagi K., 2019, *Phys. Rev. D*, 99, 043010  
 Centelles M., Roca-Maza X., Viñas X., Warda M., 2009, *Phys. Rev. Lett.*, 102, 122502  
 Chabanat E., Bonche P., Haensel P., Meyer J., Schaeffer R., 1998, *Nucl. Phys. A*, 635, 231  
 Chen W.-C., Piekarewicz J., 2014, *Phys. Rev. C*, 90, 044305  
 Ciarcelluti P., Sandin F., 2011, *Phys. Lett. B*, 695, 19–21  
 Cline J. M., Scott P., Kainulainen K., Weniger C., 2013, *Phys. Rev. D*, 88, 055025  
 Collins J. C., Perry M. J., 1975, *Phys. Rev. Lett.*, 34, 1353  
 Conrad J., 2014 ([arXiv:1411.1925](https://arxiv.org/abs/1411.1925))  
 Cromartie H. T., et al., 2019, *Nature Astronomy*, 4, 72–76  
 Đapo H., Schaefer B.-J., Wambach J., 2010, *Phys. Rev. C*, 81, 035803  
 Danielewicz P., Lee J., 2014, *Nucl. Phys. A*, 922, 1  
 Das A., Malik T., Nayak A. C., 2019, *Phys. Rev. D*, 99, 043016  
 De Lavallaz A., Fairbairn M., 2010, *Phys. Rev. D*, 81, 123521  
 Dechargé J., Gogny D., 1980, *Phys. Rev. C*, 21, 1568  
 Del Estal M., Centelles M., Viñas X., Patra S. K., 2001, *Phys. Rev. C*, 63, 024314

- Demorest P. B., Pennucci T., Ransom S. M., Roberts M. S. E., Hessels J. W. T., 2010, *Nature*, 467, 1081–1083
- Dhiman S. K., Kumar R., Agrawal B. K., 2007, *Phys. Rev. C*, 76, 045801
- Duffy L. D., van Bibber K., 2009, *New Journal of Physics*, 11, 105008
- Dutra M., Lourenço O., Sá Martins J. S., Delfino A., Stone J. R., Stevenson P. D., 2012, *Phys. Rev. C*, 85, 035201
- Einstein A., 1916, *Annalen Phys.*, 49, 769
- Ellis J., Hütsi G., Kannike K., Marzola L., Raidal M., Vaskonen V., 2018, *Phys. Rev. D*, 97, 123007
- Fatoyev F. J., Newton W. G., Xu J., Li B.-A., 2012, *Phys. Rev. C*, 86, 025804
- Fonseca E., et al., 2016, *APJ*, 832, 167
- Fortin M., Avancini S. S., Providência C., Vidaña I., 2017, *Phys. Rev. C*, 95, 065803
- Friedman J. L., Stergioulas N., 2013, *Rotating Relativistic Stars*. Cambridge Monographs on Mathematical Physics, Cambridge University Press, doi:10.1017/CBO9780511977596
- Furnstahl R. J., Price C. E., Walker G. E., 1987, *Phys. Rev. C*, 36, 2590
- Furnstahl R. J., Serot B. D., Tang H.-B., 1997, *Nucl. Phys. A*, 615, 441
- Glendenning N. K., 1985, *API*, 293, 470
- Glendenning N. K., 1992, *Phys. Rev. D*, 46, 1274
- Glendenning N. K., 1997, *Compact stars: Nuclear physics, particle physics, and general relativity*. Springer-Verlag New York
- Glendenning N. K., Schaffner-Bielich J., 1998, *Phys. Rev. Lett.*, 81, 4564
- Glendenning N. K., Schaffner-Bielich J., 1999, *Phys. Rev. C*, 60, 025803
- Gnedin O. Y., Phys. Rev. ovlev D. G., Potekhin A. Y., 2001, *MNRAS*, 324, 725
- Goldman I., Nussinov S., 1989, *Phys. Rev. D*, 40, 3221
- Guillot S., et al., 2019, *APJ*, 887, L27
- Gupta N., Arumugam P., 2012, *Phys. Rev. C*, 85, 015804
- Haensel P., Zdunik J. L., Bejger M., Lattimer J. M., 2009, *A&A*, 502, 605–610
- Hall L. J., Jedamzik K., March-Russell J., West S. M., 2010, *JHEP*, 2010, 80
- Han T., Liu Z., Su S., 2014, *JHEP*, 2014, 93
- Hessels J. W. T., Ransom S. M., Stairs I. H., Freire P. C. C., Kaspi V. M., Camilo F., 2006, *Science*, 311, 1901
- Hooper D., Wang L.-T., 2004, *Phys. Rev. D*, 69, 035001
- Horowitz C. J., et al., 2014, *Journal of Physics G: Nuclear and Particle Physics*, 41, 093001
- Ivanytskyi O., Sagun V., Lopes I., 2019 (arXiv:1910.09925)
- Jha T. K., Mishra H., Sreekanth V., 2008, *Phys. Rev. C*, 77, 045801
- Kaaret P., et al., 2007, *APJ*, 657, L97
- Kaplan D., Nelson A., 1988, *Nucl. Phys. A*, 479, 273
- Kojo T., Powell P. D., Song Y., Baym G., 2015, *Phys. Rev. D*, 91, 045003
- Koliogiannis P. S., Moustakidis C. C., 2020, *Phys. Rev. C*, 101, 015805
- Komatsu H., Eriguchi Y., Hachisu I., 1989a, *MNRAS*, 237, 355
- Komatsu H., Eriguchi Y., Hachisu I., 1989b, *MNRAS*, 239, 153
- Kouvaris C., 2008, *Phys. Rev. D*, 77, 023006
- Kouvaris C., Tinyakov P., 2010, *Phys. Rev. D*, 82, 063531
- Kouvaris C., Tinyakov P., 2011, *Phys. Rev. D*, 83, 083512
- Krastev P. G., Li B., Worley A., 2008, *APJ*, 676, 1170–1177
- Kubis S., Kutschera M., 1997, *Phys. Lett. B*, 399, 191–195
- Kumar B., Landry P., 2019, *Phys. Rev. D*, 99, 123026
- Kumar B., Biswal S. K., Patra S. K., 2017, *Phys. Rev. C*, 95, 015801
- Kumar B., Patra S. K., Agrawal B. K., 2018, *Phys. Rev. C*, 97, 045806
- Kumar A., Das H. C., Biswal S. K., Kumar B., Patra S. K., 2020 (arXiv:2005.08320)
- Lalazissis G. A., König J., Ring P., 1997, *Phys. Rev. C*, 55, 540
- Landry P., Kumar B., 2018, *APJ*, 868, L22
- Lattimer J. M., Prakash M., 2000, *Physics Reports*, 333-334, 121–146
- Lattimer J. M., Prakash M., 2004, *Science*, 304, 536
- Leung S.-C., Chu M.-C., Lin L.-M., 2011, *Phys. Rev. D*, 84, 107301
- Li A., Huang F., Xu R.-X., 2012, *Astroparticle Phys.*, 37, 70–74
- Li B.-A., Krastev P. G., Wen D.-H., Zhang N.-B., 2019, *EPJ A*, 55
- Malik T., Alam N., Fortin M., Providência C., Agrawal B. K., Jha T. K., Kumar B., Patra S. K., 2018, *Phys. Rev. C*, 98, 035804
- Martin S. P., 1998, *A Supersymmetry Primer*. pp 1–98, doi:10.1142/9789812839657\_0001
- Matsui T., 1981, *Nucl. Phys. A*, 370, 365
- McLerran L., Reddy S., 2019, *Phys. Rev. Lett.*, 122, 122701
- Mellinger R., Weber F., Spinella W., Contrera G., Orsaria M., 2017, *Universe*, 3, 5
- Miller L. D., Green A. E. S., 1972, *Phys. Rev. C*, 5, 241
- Miller M. C., et al., 2019, *APJ*, 887, L24
- Moustakidis C. C., Gaitanos T., Margaritis C., Lalazissis G. A., 2017, *Phys. Rev. C*, 95, 045801
- Newton W. G., Gearheart M., Li B.-A., 2012, *APJ Suppl. Series*, 204, 9
- Oppenheimer J. R., Volkoff G. M., 1939, *Phys. Rev.*, 55, 374
- Orsaria M., Rodrigues H., Weber F., Contrera G. A., 2014, *Phys. Rev. C*, 89, 015806
- Page D., Lattimer J. M., Prakash M., Steiner A. W., 2004, *APJ Suppl. Series*, 155, 623–650
- Pal S., Bandyopadhyay D., Greiner W., 2000, *Nucl. Phys. A*, 674, 553–577
- Panotopoulos G., Lopes I., 2017, *Phys. Rev. D*, 96, 083004
- Paschalidis V., Stergioulas N., 2017, *Living Rev. Relativ.*, 20, 7
- Quddus A., Panotopoulos G., Kumar B., Ahmad S., Patra S. K., 2019 (arXiv:1902.00929)
- Raaijmakers G., et al., 2019, *Astrophys. J*, 887, L22
- Rashdan M., 2001, *Phys. Rev. C*, 63, 044303
- Reinhard P. G., 1988, *Z. Phys. A Atomic Nuclei*, 329, 257
- Rhoades C. E., Ruffini R., 1974, *Phys. Rev. Lett.*, 32, 324
- Riley T. E., et al., 2019, *APJ*, 887, L21
- Ruppin F., Billard J., Figueroa-Feliciano E., Strigari L., 2014, *Phys. Rev. D*, 90, 083510
- Sandin F., Ciarcelluti P., 2009, *Astroparticle Phys.*, 32, 278–284
- Schaffner J., Mishustin I. N., 1996, *Phys. Rev. C*, 53, 1416
- Schulze H.-J., Polls A., Ramos A., Vidaña I., 2006, *Phys. Rev. C*, 73, 058801
- Serot B. D., Walecka J. D., 1986, *Adv. Nucl. Phys.*, 16, 1
- Sharma B. K., Jha T. K., 2009 (arXiv:0905.1549)
- Sharma B. K., Panda P. K., Patra S. K., 2007, *Phys. Rev. C*, 75, 035808
- Singh S. K., Bhuyan M., Panda P. K., Patra S. K., 2013, *Journal of Physics G: Nuclear and Particle Physics*, 40, 085104
- Skyrme T. H. R., 1956, *The Philosophical Magazine: A Journal of Theoretical Experimental and Applied Physics*, 1, 1043
- Skyrme T., 1958, *Nuclear Physics*, 9, 615
- Steiner A. W., Gandolfi S., 2012, *Phys. Rev. Lett.*, 108, 081102
- Stergioulas N., 2003, *Living Rev. Relativ.*, 6, 3
- Stergioulas N., Morsink S., 1999, UWM Physics Department
- Stone J., Reinhard P.-G., 2007, *Progress in Particle and Nuclear Physics*, 58, 587–657
- Stone J. R., Stone N. J., Moszkowski S. A., 2014, *Phys. Rev. C*, 89, 044316
- Tolman R. C., 1939, *Phys. Rev.*, 55, 364
- Vautherin D., Brink D. M., 1972, *Phys. Rev. C*, 5, 626
- Walecka J., 1974, *Ann. Phys.*, 83, 491
- Worley A., Krastev P. G., Li B.-A., 2008, *APJ*, 685, 390
- Xiang Q.-F., Jiang W.-Z., Zhang D.-R., Yang R.-Y., 2014, *Phys. Rev. C*, 89, 025803
- Xu C., Li B.-A., Chen L.-W., 2010, *Phys. Rev. C*, 82, 054607
- Yakovlev D., Pethick C., 2004, *Ann. Rev. A&A*, 42, 169–210
- Yakovlev D., Gnedin O., Gusakov M., Kaminker A., Levenfish K., Potekhin A., 2005, *Nucl. Phys. A*, 752, 590–599
- Yakovlev D. G., Ho W. C. G., Shternin P. S., Heinke C. O., Potekhin A. Y., 2010, *MNRAS*, 411, 1977–1988
- Young R. D., 2012, *Proceedings of Science*, 164
- Zimmerman J., Carson Z., Schumacher K., Steiner A. W., Yagi K., 2020 (arXiv:2002.03210)
- Zwicky F., 2009, *General Relativity and Gravitation*, 41, 207